Decomposition of CH_2O by Lanthanum: A Theoretical Study

Guozhen Zhang, Zhen Hua Li, Wen-Ning Wang, and Kang-Nian Fan*

Department of Chemistry, Shanghai Key Laboratory of Molecular Catalysts and Innovative Materials, Fudan University, Shanghai 200433, P. R. China

Received: July 8, 2007; In Final Form: September 12, 2007

This work aims to investigate the reaction mechanism of lanthanum atom with formaldehyde in the gas phase using density functional theory and coupled cluster calculations. The results indicate that the minimum energy pathway, similar to the reactions of its neighboring yttrium with formaldehyde, is the formation of the η^2-formaldehyde−metal complex followed by two C−H insertions which leads to metal dihydrides and carbon monoxide. The competing pathway producing a metal−carbonyl compound and hydrogen molecule favors a high-spin state and thus involves a spin conversion from doublet state to quartet state. The crossing region of the doublet and quartet potential energy surfaces (PES) has been estimated by a simple approach as proposed by Yoshizawa et al. Less favorable pathways leading to metal monoxide and carbene radical by C−O insertion as well as formyllanthanum by single C−H insertion are also studied. Compared with the CCSD(T) method, the BP86 method tends to overestimate the binding energies of the d-rich compounds, though the two methods qualitatively agree well on the reaction mechanism. Finally, the $(n - 1)d^1ns^2$ to $(n - 1)d^2ns^1$ promotion effect is proposed to account for the difference in the formation mechanism of the metal−carbonyl compounds LaCO and YCO, which may also extend to the reactions of formaldehyde with other "general" group III rare earth elements including Sc, Ce, Gd, and Lu.

1. Introduction

Formaldehyde, the simplest carbonyl-containing organic molecule, is one of the most important compounds in organic reactions both for fundamental scientific reasons and for many practical applications involving organic synthesis, catalysis, combustion, and atmospheric chemistry.[1−3]

It is well-established that formaldehyde is the product of carbon monoxide hydrogenation or methanol dehydrogenation. As formaldehyde is the key intermediate of these catalytic reaction chains, its possible transformations are catalytic reactions of interest.[4] In addition, formaldehyde is a notorious health hazard.[5] To study its degradation via chemical reactions would help us to design effective means of eliminating it from air. Compared to its activity in other common hydrocarbons, the C−H bond in formaldehyde is more active. For example, previous study[6] has shown that its C−H dissociation energy in CH_2O is remarkably smaller than that for both unsaturated species like ethylene and acetylene and saturated hydrocarbons like ethane. This may imply some new characteristics associated with the ambient π-electron about the C═O double bond.[7]

Herein we focus on reactions between formaldehyde and transition metals, since catalytic hydrogenation of carbon monoxide as well as C−H activation of aldehyde and ketone are usually promoted by metal-bearing catalysts. It is well-documented that metal−formaldehyde complexes[8] [$M(CH_2O)$] are of extensive existence in reactions involving metal compounds and small organic molecules (including methane, methanol, formaldehyde, acetone, fatty acids, etc.). Furthermore, $M(CH_2O)$ is a simplified yet important model for both catalytic disassociation of formaldehyde and catalytic hydrogenation of carbon monoxide in the reverse direction.[9,10] Their chemistry involving both C−O activation and C−H activation, together with formation of a bimetallic bridged compound ($M-CH_2O-M'$), mainly takes place in three sorts of conditions: catalysis on surfaces of a solid phase; organometallic reactions in a liquid phase; radical reactions in a gas phase. In this paper we only discuss reactions in the gas phase, the simplest case. The study in the gas phase can provide useful information on reaction mechanisms toward a full understanding of the practical reactions.

In previous studies involving [$M(CH_2O)$] in the gas phase, both experimental and theoretical work have paid much attention to the late transition metals (such as Ni, Co, Cu, Zn, Rh, Pd, and Ag); on the other hand, the reactions between formaldehyde and lanthanide belonging to early transition metals have not drawn much attention. However, some lanthanides (such as La) have been reported to function as a key promoters[11] in catalytic reactions of oxidation of methane and dehydrogenation of methanol. Thus, it is necessary to study $LaCH_2O$ and its related transformations. Recently, Stauffer[7] et al. have reported the reaction between formaldehyde and yttrium, which is lanthanum's neighbor in group III. The detailed reaction mechanism, as proposed by Bayse,[12] involves initial formation of the $Y-CH_2O$ complex followed by two C−H insertions which branch out to competing pathways to decarbonyl products and dehydrogenated products. Because the extremely high reaction barrier for dehydrogenation is believed to hinder the production of $YCO(^2\Pi)$, an alternative pathway for the second C−H insertion which involves a weak (η^2-H_2)YCO complex and subsequently direct dehydrogenation has also been proposed by Bayse. As for La, although the electron configuration ($5d^16s^2$) is similar to that for Y ($4d^15s^2$), it is much easier for La to promote an electron from the *n*s to $(n - 1)$d orbital (0.33 eV) than for Y (1.36 eV).[13] The resulting $(n - 1)d^2ns^1$ configuration has been regarded to be favorable in activation of hydrocar-

* To whom correspondence should be addressed. E-mail: knfan@fudan.edu.cn. Fax: +86-21-65642978.

10.1021/jp0753169 CCC: $37.00
Published on Web 10/30/2007

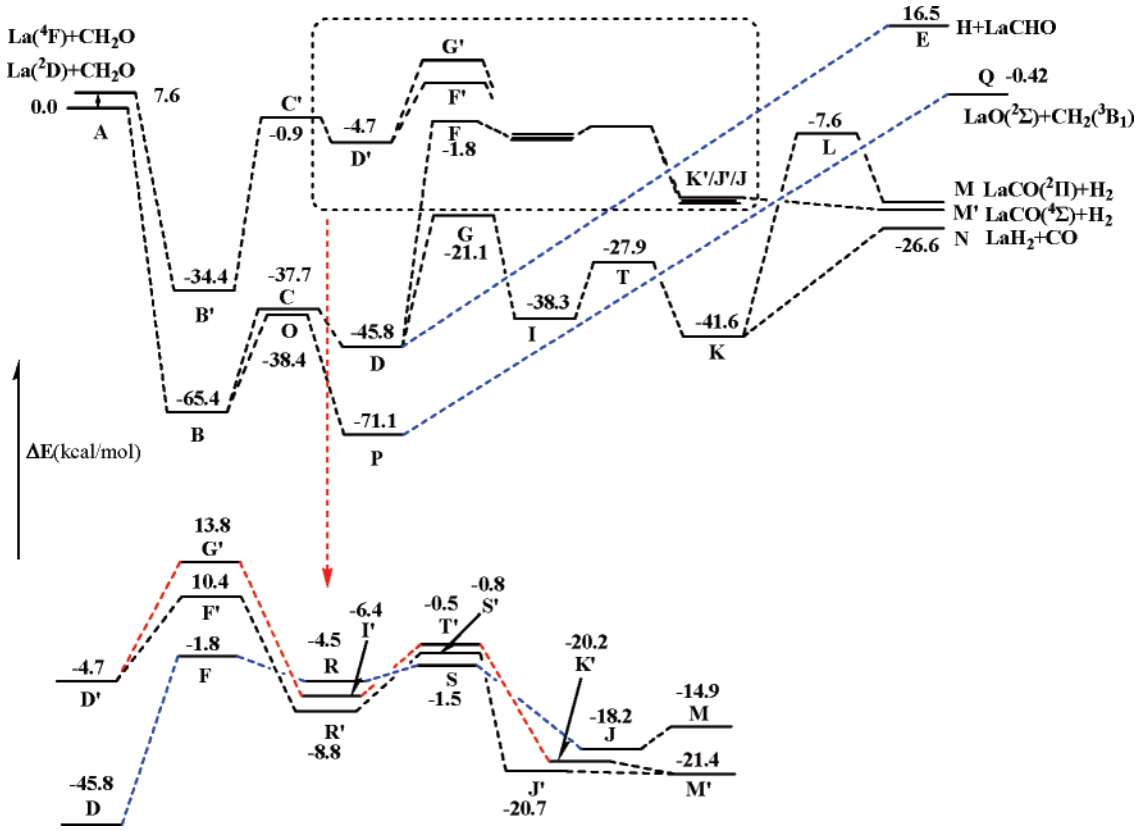

Figure 1. Potential energy profiles for the reaction between La and CH_2O calculated at the CCSD(T)/SDD/cc-PVTZ level.

bons.[14] It is thus expected that the reaction between La and CH_2O may have some new features. What is more, the ground state of LaCO is assigned to be a $^4\Sigma$ state rather than $^2\Pi$ state,[15] indicating the dehydrogenation of $LaCH_2O$ will be different from that of YCH_2O.

To the best of our knowledge, no studies on the reaction of the neutral lanthanum atom and formaldehyde in the gas phase have been reported. Here we present a computational study on this important model reaction. This study could also help to depict a general trend on reactions of formaldehyde and "general" group III elements (including Sc, Y, La, Ce, Gd, and Lu).

2. Computational Details

Density functional theory (DFT) has been proven to be a suitable choice for moderately accurate studies of small molecules in the gas phase at a low cost.[16] Thus, our scheme is to sketch the reaction coordinate first at a DFT level, followed by accurate couple cluster calculations for energy correction.

All DFT calculations were performed using the Amsterdam density functional (ADF 2006.01) program.[17] The functional employed in this study is Becke−Perdew (BP86), which combines Becke's 1988 exchange functional (B)[18] with Perdew's 1986 gradient corrected correlation functional (P86).[19] Although older than many other popular density functionals, it is well-documented that BP86 performs well in transition-metal-containing systems.[20] To reduce computing cost, a frozen core approximation was applied to the 1s of C and O and 1s−4d of La. The valence orbitals of C, H, O, and La were represented with a basis set of TZV quality and two polarization functions.[21] The scalar-relativistic corrections were carried out by the zero-order regular approximation (ZORA) method.[22] Geometries of all species were fully optimized, using restricted Kohn−Sham orbitals[23] for closed-shell systems and unrestricted ones for open-shell systems. Vibrational frequencies and corresponding zero-point energies (ZPE) were calculated with ADF for each stationary point. To further analyze reaction path characters, intrinsic reaction coordinate (IRC)[24] calculations were carried out in both forward and backward directions from transition states. Then, single point calculation was carried out for each stationary point by the same DFT method with a larger QZ4P[21] basis set for more accurate energies.

On the basis of the geometries obtained from DFT calculations at the ZORA-BP86/TZ2P level, single-point energy calculations were performed with the GAUSSIAN 03 program[25] using the CCSD(T)[26] method. Herein the relativistic effect for La was described using a relativistic energy-consistent small-core pseudopotential (Dolg's SC-ECP) developed by the Stuttgart−Dresden group (referred as SDD).[27] The 1s−3d shells were included in the pseudopotential core, while all shells with a main quantum number larger than 3 were treated explicitly. Gaussian (14s13p10d8f6g)/[10s8p5d4f3g] segmented contraction valence basis sets[28] were applied in conjunction with Dolg's SC-ECP. For light elements (C, H, and O), the cc-PVTZ basis set[29] was used, as suggested by de Jong[30] et al.

Energies of all stationary points in the reaction coordinate are relative to the total energy of La(^{2}D) + CH_2O. It is still a challenging issue to compute the atomic reference energy of La on the basis of a single-reference determinant wave function. Here we used Baerend's method[31] to evaluate the ground state of La at the DFT level. At the CCSD(T) level, a symmetry-broken wave function was used to evaluate the atomic reference energy. Energy data within the text below refer to the results of CCSD(T) calculations unless otherwise specified.

3. Results and Discussion

The energy profiles for the reaction between lanthanum and formaldehyde are shown in Figure 1. The energies (including

TABLE 1: Relative Energies (in kcal mol^{-1}) of All Stationary Points with Respect to Reactants La(^{2}D) + CH_2O at Different Levels

	ZORA-BP86/ TZ2P		ZORA-BP86/ QZ4P		CCSD(T)/SDD/ cc-PVTZ[a]	
species	**doublet**	**quartet**	**doublet**	**quartet**	**doublet**	**quartet**
B	−77.5	−47.6	−79.8	−49.4	−65.4	−34.4
C	−51.1	−16.5	−53.0	−18.2	−37.7	−0.9
D	−59.7	−18.0	−61.7	−19.6	−45.8	−4.7
E	2.5		0.60		16.5	
G	−34.9	−6.8	−37.6	−9.2	−21.1	13.8
I	−46.7	−21.1	−47.9	−22.7	−38.3	−6.4
T	−41.9	−18.5	−43.1	−20.1	−27.9	−0.5
K	−52.6	−35.6	−53.7	−37.2	−41.6	−20.2
L	−27.4		−28.7		−7.6	
N	−28.4		−29.2		−26.6	
F	−19.2	−11.3	−21.2	−13.2	−1.8	10.4
R	−19.9	−22.9	−22.1	−24.1	−4.5	−8.8
S	−19.0	−20.3	−21.0	−22.0	−1.5	−0.8
J	−35.4	−35.0	−37.2	−35.8	−18.2	−20.7
M	−22.7	−34.9	−23.8	−36.2	−14.9	−21.4
O	−55.4		−58.5		−38.4	
P	−84.5		−87.8		−71.1	
Q	−4.9	−20.3	−8.7	−23.7	−0.42	−10.2

[a] Small core SDD basis set is used for La, and the cc-PVTZ basis set is used for C, H, and O.

ZPE correction at the DFT level) relative to La(^{2}D) + CH_2O are listed in Table 1. Mulliken charges, spin densities, and atomic orbital populations of each stationary point are listed in Table 2 for the doublet potential energy surface (PES) and Table 3 for the quartet PES. Geometries and selected parameters of stationary points are presented in Figure 2.

As shown in Figure 1, the reaction between La(^{2}D) + CH_2O involves initial formation of the La−H_2CO complex (**B**) followed by two C−H insertions to form carbonyldihydridolanthanum (**K**) or carbonyl(η^2-dihydrogen)lanthanum (**J**). Two sets of products can be produced: one is lanthanum dihydride (LaH_2) formed by the loss of CO, and the other is lanthanum carbonyl **(**LaCO**)** formed by the loss of H_2. The former is favorable in both thermodynamics and kinetics.

The above reaction mechanism for doublet PES is similar to that of Y(^{2}D) + CH_2O.[12] However, the formation of LaCO may be more complicated than that of YCO because YCO may only involve a doublet state ($^2\Pi$), while LaCO involves a doublet state ($^2\Pi$) as well as quartet state ($^4\Sigma$). Consequently, it is necessary to analyze both doublet and quartet PES to rationalize spin conversion from the former to latter, which leads to the ground state of LaCO($^4\Sigma$). Besides, there are two possible products of theoretical interest: one is complex H_2CLaO (**P**), which can dissociate into carbene and LaO, and the other is LaCHO (**E**) after loss of one hydrogen atom in complex HLaCHO (**D**). In the following two sections, we will discuss them in detail.

3.1. DFT vs CCSD(T): Comparison of Relative Energies. CCSD(T) results are generally regarded as benchmarks for small-size molecules.[16] As shown in Table 1, bonding energies

TABLE 2: Mulliken Charges, Spin Densities, and Populations for La(^{2}D) + CH_2O Stationary Points at the BP86/TZ2P Level with All Values in au

	Mulliken charge (spin density)[a]					atomic orbital populatn of La			
species	La	C	O	H	H[b]	6s	6p	5d	4f
CH_2O		0.80	−0.51	−0.15	−0.15				
B	0.59 (1.01)	0.41	−0.60	−0.19	−0.19	0.810	0.057	1.290	0.256
C	0.58 (0.87)	0.51 (0.13)	−0.57	−0.24	−0.27	0.654	0.029	1.511	0.231
D	0.91 (0.38)	0.30 (0.54)	−0.59 (0.13)	−0.24	−0.38	0.292	0.031	1.508	0.261
G	0.97 (0.35)	0.08 (0.58)	−0.56	−0.14	−0.35	0.248	0.042	1.447	0.289
I	1.06 (0.41)	0.14 (0.52)	−0.46	−0.37	−0.37	0.261	0.116	1.360	0.208
T	0.99 (0.48)	0.14 (0.40)	−0.42 (0.14)	−0.35	−0.35	0.294	0.084	1.427	0.204
K	0.97 (0.53)	0.11 (0.36)	−0.35 (0.13)	−0.37	−0.37	0.241	0.096	1.509	0.186
L	0.60 (0.64)	0.10 (0.23)	−0.37 (0.13)	−0.17	−0.17	0.255	0.049	1.924	0.167
M	0.14 (0.56)	0.19 (0.33)	−0.33 (0.11)			1.274	0.057	1.428	0.100
N	0.68 (1.00)	−0.34	−0.34			0.738	0.053	1.404	0.128
F	0.53 (0.85)	0.09 (0.13)	−0.53	0.15	−0.25	0.211	0.062	2.009	0.188
R	0.51 (0.41)	0.08 (0.44)	−0.51 (0.11)	0.03	−0.10	0.413	0.054	1.828	0.192
S	0.46 (0.61)	0.14 (0.30)	−0.49	0.02	−0.12	0.390	0.029	1.951	0.164
J	0.35 (0.77)	0.17 (0.15)	−0.42 (0.11)	0.07	−0.16	0.555	0.010	1.931	0.156
O	0.81 (0.59)	0.03 (0.42)	−0.58	−0.13	−0.13	0.516	0.071	1.260	0.338
P	1.10	−0.13 (0.91)	−0.67	−0.17	−0.14	0.115	0.000	1.435	0.356

[a] Spin densities are in parentheses, and only absolute values larger than 0.1 are presented. [b] The first hydrogen atom that transfers.

TABLE 3: Mulliken Charges, Spin Densities, and Populations for La(^{4}F) + CH_2O Stationary Points at the BP86/TZ2P Level with All Values in au

	Mulliken charge (spin density)[a]					atomic orbital populatn of La			
species	La	C	O	H	H[b]	6s	6p	5d	4f
CH_2O		0.80	−0.51	−0.15	−0.15				
B′	0.36 (2.18)	0.61 (0.85)	−0.63	−0.17	−0.17	0.870	0.051	1.564	0.157
C′	0.63 (1.40)	0.36 (1.19)	−0.57 (0.28)	−0.15	−0.27	0.700	0.071	1.405	0.195
D′	0.71 (1.32)	0.31 (1.27)	−0.55 (0.29)	−0.12	−0.34	0.701	0.098	1.300	0.196
F′	0.50 (1.61)	0.21 (1.12)	−0.52 (0.22)	0.08	−0.27	0.715	0.078	1.456	0.247
R′	0.30(2.20)	0.14 (0.62)	−0.47 (0.10)	0.02	0.02	0.749	0.127	1.703	0.126
S′	0.37 (2.17)	0.15 ((0.48)	−0.45(0.18)	−0.02	−0.03	0.53	0.110	1.843	0.149
J′	0.18 (2.39)	0.17 (0.37)	−0.38 (0.20)	0.01	0.01	0.848	0.058	1.828	0.084
G′	0.55 (1.70)	0.20 (0.84)	−0.51 (0.30)	0.01	−0.25 (0.11)	0.651	0.124	1.447	0.233
I′	0.32 (2.17)	0.12 (0.62)	−0.46 (0.13)	0.02	0.00	0.792	0.160	1.571	0.130
T′	0.30 (2.23)	0.12 (0.48)	−0.44 (0.22)	0.04	−0.01	0.737	0.203	1.614	0.147
K′	0.23 (2.30)	0.15 (0.40)	−0.39 (0.22)	0.05	−0.04	0.772	0.078	1.803	0.120
M′	0.22 (2.36)	0.17 (0.40)	−0.40 (0.24)			0.898	0.044	1.736	0.098

[a] Spin densities are in parentheses, and only absolute values larger than 0.1 are presented. [b] The first hydrogen atom that transfers.

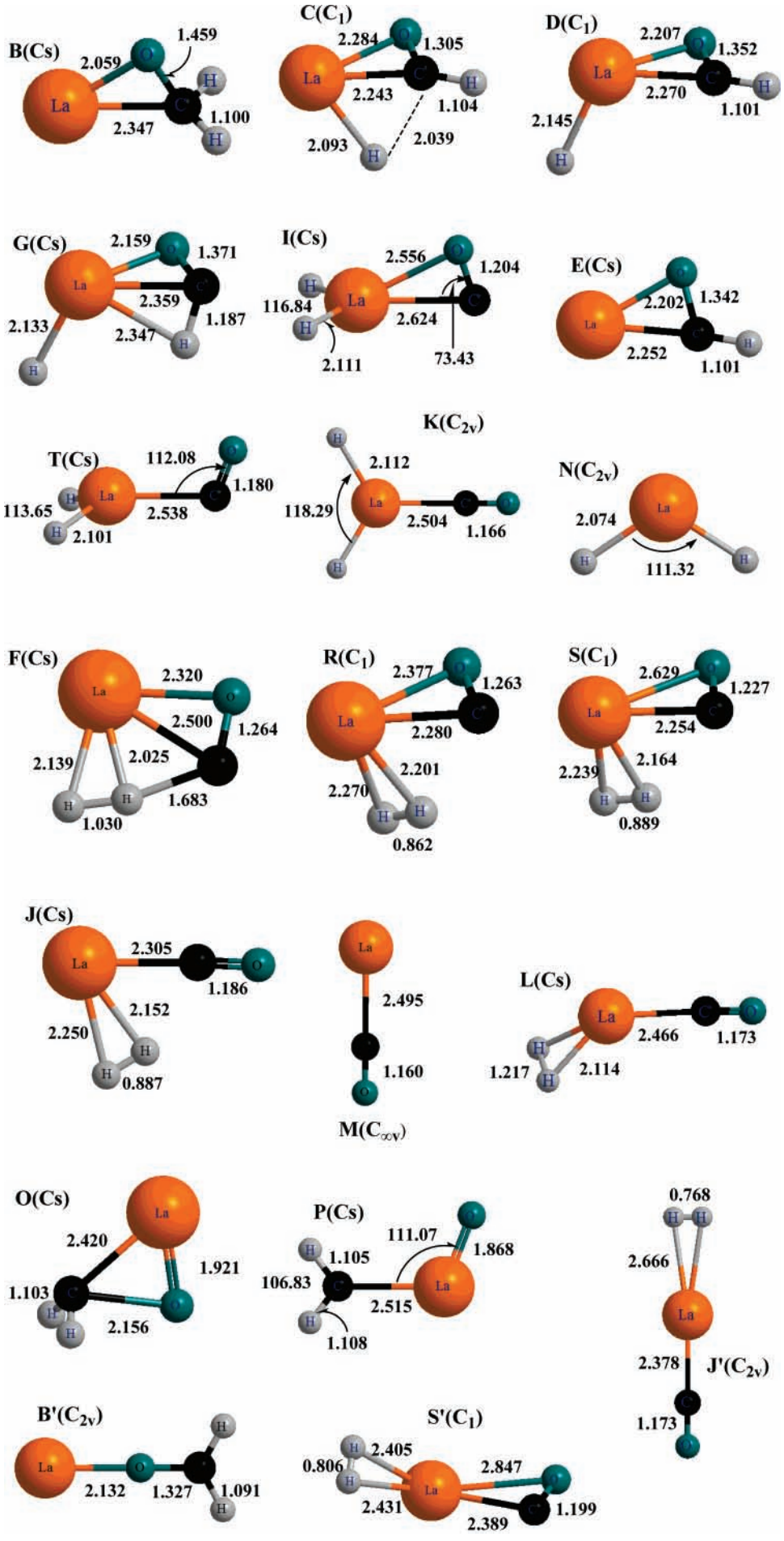
B(Cs)
1.459
2.059
1.100
2.347
C(C1)
2.284
1.305
2.243
1.104
2.093
2.039
D(C1)
2.207
1.352
2.270
1.101
2.145
G(Cs)
2.159
1.371
2.359
1.187
2.133
2.347
I(Cs)
2.556
1.204
116.84
2.624
2.111
73.43
E(Cs)
2.202
1.342
2.252
1.101
T(Cs)
112.08
1.180
113.65
2.538
2.101
K(C2v)
2.112
118.29
2.504
1.166
N(C2v)
2.074
111.32
F(Cs)
2.320
2.500
1.264
2.139
2.025
1.683
1.030
R(C1)
2.377
1.263
2.280
2.201
2.270
0.862
S(C1)
2.629
1.227
2.254
2.164
2.239
0.889
J(Cs)
2.305
1.186
2.152
2.250
0.887
2.495
1.160
M(C∞v)
L(Cs)
2.466
1.173
1.217
2.114
O(Cs)
2.420
1.921
1.103
2.156
P(Cs)
111.07
1.868
1.105
106.83
2.515
1.108
0.768
2.666
2.378
J'(C2v)
1.173
B'(C2v)
2.132
1.327
1.091
S'(C1)
0.806
2.405
2.847
2.431
1.199
2.389

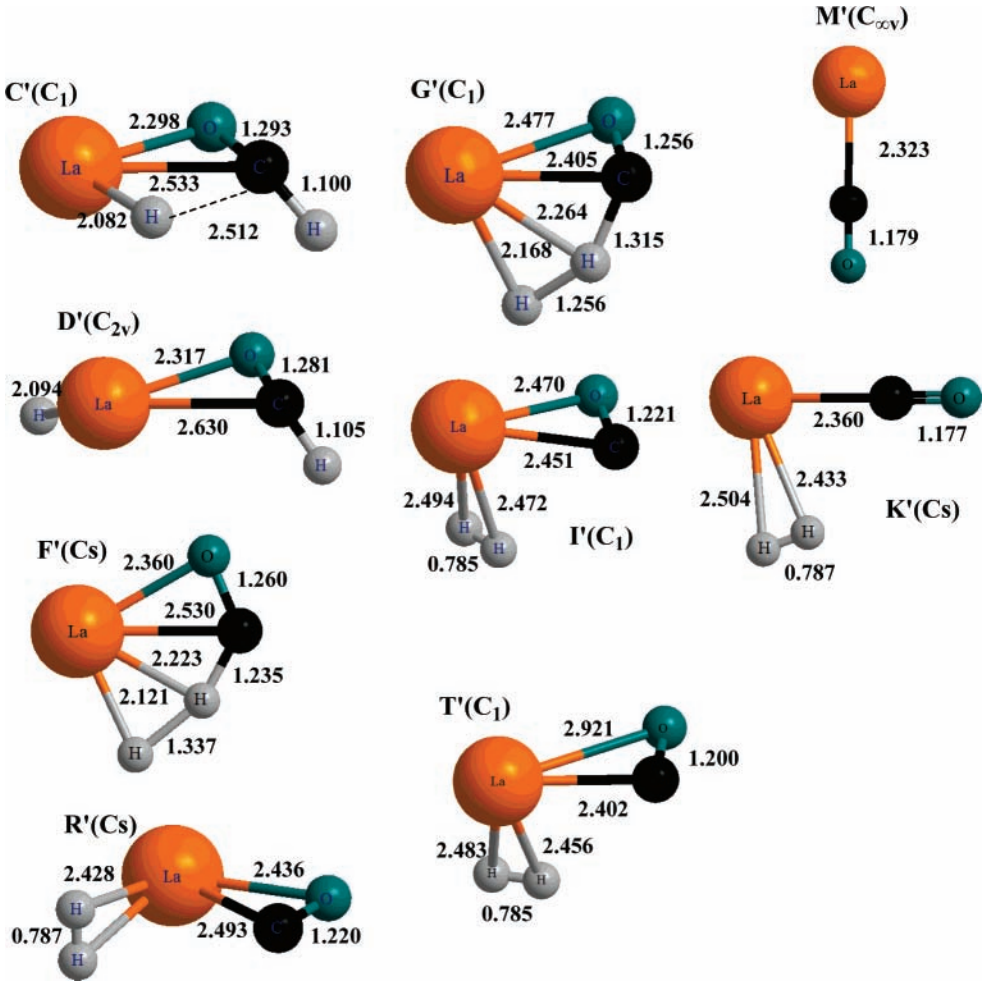

Figure 2. Selected geometric parameters for stationary points on the reaction coordinate of lanthanum and formaldehyde. Bond lengths are given in Å, and the point group for each species is given in parentheses.

for open-shell species at the ZORA-BP86/QZ4P level are generally 15.0 ± 5.0 kcal mol^{-1} larger than those at the CCSD(T)/SDD/cc-PVTZ level. Since the error bar of the QZ4P basis set is less than 1.0 kcal mol^{-1},[21] the basis set error does not account for the error discussed here. Thus, the main error source should be from the functional we used. It is well-documented that pure-DFT methods are prone to overestimate bonding energies and underestimate barrier heights.[32] Meanwhile, it is notable that reaction trends are nearly the same for both DFT and CCSD(T) levels. The above two aspects indicate that initial geometric optimization at the DFT level followed by energy corrections at the CCSD(T) level is an appropriate choice for reactions discussed in this paper.

3.2. Reaction Pathway to $LaH_2 + CO$. At the initial reaction step, the doublet lanthanum atom attaches to formaldehyde without an energy barrier, forming a π-complex **B** which is −65.4 kcal mol^{-1} lower than the reactants. The high exothermicity of the reaction may be due to the highly oxophilic[33] character of lanthanum. **B** has the structure of the so-called "metallepoxide", like its counterpart YCH_2O.[12] Because both C and O have some bonding with La, the C−O bond (1.459 Å) is weakened and becomes a single bond. The electron transfer from La to C may also, to some extent, stabilize this complex by decreasing the positive charge on C. However, the unpaired electron still locates on La as indicated by spin density distribution, which can facilitate the subsequent C−H bond dissociation.

At the second step, La inserts into one C−H bond forming intermediate (IM) **D** via transition state **C** with an energy barrier of 27.7 kcal mol^{-1}. To facilitate the C−H insertion by La, the CH_2O moiety in IM **D** needs to be twisted by about 70° around the C−O bond, concerted by breaking of the C−H bond (2.039 Å in TS **C**) and forming of the La−H bond (2.093 Å in TS **C**). The Mulliken charge distribution as presented in Table 2 shows that electron continues to flow from La to C and the transferring H, causing the spin density on La to decrease remarkably.

There are three possible pathways from IM **D** (see Figure 1) leading to three types of products, which are dehydrogen product **E**, dedihydrogen product **M**, and decarbonyl product **N**. Among the three pathways, decarbonyl pathway is the most favorable one for it overcomes the lowest energy barriers and releases the most heat.

Transforming from **D** to **M** involves two transition states (**G** and **T**) and two intermediates (**I** and **K**). Both TS **C** and TS **G** lead to H-transfer, but the patterns of C−H bond activation are much different. From the view of geometric change, the breaking C−H bond (2.039 Å) in TS **C** is about two times the length of the normal C−H bond, while its counterpart (1.187 Å) in TS **G** is just slightly longer than the normal C−H bond. From the view of charge distribution, the former, involving a substantial increase of positive charge on La, can be considered as an oxidative addition of metal, while the latter, resulting in little change of charge on La and some charge transfer from leaving H to C, can be considered as a hydride shift. The difference in natures of two C−H insertions may be due to the deficiency of 5d electrons of La, similar to Y.[12]

IM **I**, which has not been located in the previous study of Y + CH_2O, is a direct product from IM **D** via TS **G** as confirmed by IRC analysis. The C−O bond in **I** is 1.204 Å, slightly shorter than a typical side-on carbonyl ligand. It can easily convert to a terminal carbonyl ligand via TS **T**, forming a more stable IM **K**.

IM **K**, formed from the LaH_2 moiety and CO moiety, has a C_{2v} symmetry. Meanwhile, the geometry of the LaCO moiety (La−C, 2.504 Å; C−O, 1.166 Å) is close to that of isolated doublet LaCO (La−C, 2.495 Å; C−O, 1.160 Å). Thus, this complex may be viewed as either carbonyl dihydridolanthanum or carbonyllanthanum dihydride. Consequently, there are two competing ways of decomposition for **K**: loss of CO; loss of H_2. The decarbonyl products are 26.6 kcal mol^{-1} below the reactants, more favorable in energy. The loss of carbonyl is expected to be barrierless, similar to that of the Y + CH_2O reaction.[12] The resulting lanthanum dihydride is in the $^2A_1$ state. The calculated LaH stretching frequencies of LaH_2 are 1330 and 1365 cm^{-1}, close to experimental values[34] of 1283 and 1321 cm^{-1}.

3.3. Reaction Pathways to LaCO + H_2. As mentioned above, the dehydrogenation pathways are more complicated, since the quartet state rather than doublet state is the ground state of LaCO. In line with previous study,[15] our calculation results also indicate that LaCO($^4\Sigma$) is lower than LaCO($^2\Pi$) in energy by 12.4 kcal mol^{-1} at the ZORA-BP86/QZ4P level while it is lower by 6.5 kcal mol^{-1} at the CCSD(T) level. In addition, the computed ν(CO) frequency in LaCO($^4\Sigma$) is 1799 cm^{-1}, in excellent agreement with the experimental value of 1772.7 cm^{-1},[35] while the ν(CO) frequency in LaCO($^2\Pi$) is 1918 cm^{-1}, remarkably larger than the observed value in the experiment. Therefore, we must investigate quartet PES as well as doublet PES to manifest a reasonable reaction mechanism for the production of LaCO.

3.3.1. Doublet LaCO. The first pathway leading to H_2 and LaCO ($^2\Pi$) is the decomposition of **K** via TS **L** with an energy barrier of 34.0 kcal mol^{-1}. **L** is still below reactants by −7.6 kcal mol^{-1}, and the barrier from **K** to **L** is substantially lower than the corresponding barrier in the Y + CH_2O reaction. The reason for the difference should be investigated through changes in electronic structures underlined in geometric changes. It is expectable that the similarity in the electron configuration of H_2LaCO and H_2YCO can lead to the similarity in the electron redistribution process when losing the H_2 moiety. Both La and Y bond with H atom via an sd hybrid orbital. When the M−H (M = La, Y) bond dissociates, the electron contributed by the metal atom will flow back to its *n*s orbital. This is regarded by Bayse[12] as a forbidden process since it involves jumping a pair of electrons from a π-type orbital to σ-type orbital on Y and thus requires a high energy barrier (47.3 kcal mol^{-1} at the CASPT2 level). In comparison, this energy barrier (from **K** to **L**) for La + CH_2O is 34.0 kcal mol^{-1}. Since La has a much smaller promotion energy for $ns \rightarrow (n-1)d$ excitation, it is probable that interconversions between s^2d^1 and s^1d^2 subconfigurations are much easier for La, leading to a lower barrier for this "forbidden" process on H_2LaCO. On the basis of this inference, we argue that it is not impossible that the dehydrogenation barrier for H_2LaCO is remarkably lower than the similar barrier for H_2YCO. We hope that our argument could provide ground work toward full understanding of this complicated dehydrogenation reaction.

The second pathway is from **D** to **R** and then to **J** and then the loss of H_2. As mentioned above, the second C−H bond is broken by La in terms of H-transfer. The resulting intermediate is either $H_2La(\eta^2\text{-CO})$ (**I**) if this H atom bonds with a La atom or $(\eta^2\text{-H}_2)La(\eta^2\text{-CO})$ (**R**) if this H bonds with the other H atom. IM **R** is a weakly bound complex between LaCO and H_2. Our IRC calculation[36] indicates that the two H atoms first rotate into the La−C−O plane before they approach each other. The formation of the H−H bond (1.030 Å) accompanies the breaking of the C−H the bond (1.683 Å), first resulting in a planar complex of η^2-carbonyl(η^2-dihydrogen)lanthanum. Due to the flexibility of the H_2 moiety, the complex can adopt a foldinglike conformation (**R**) by the swing of the H_2 ligand before converting into IM **J**. The side-on carbonyl ligand turns into an end-on one, overcoming an energy barrier of only 3.0 kcal mol^{-1}. The H−H distance (0.887 Å) in **J** is close to that of free H_2 (0.749 Å). Since H_2 is a good leaving group, **J** can decompose into doublet LaCO and H_2 easily. In addition, the H_2 moiety in **R** may also leave directly, producing doublet La(η^2-CO). This side-on carbonyl complex will eventually convert into end-on carbonyl complex because the former is less stable than the latter.[15]

3.3.2. Quartet LaCO. In this subsection we will discuss the loss of H_2 on the quartet PES. The capital letters with a prime represent the stationary points on the quartet PES.

The Mulliken population data (in Tables 2 and 3) indicate that, throughout the reaction, the 5d population of La is around 1.50 in both doublet and quartet states while the 6s population is obviously higher in the quartet state than in the doublet state. These trends reflect similarities and differences of reactions in two spin states. On one hand, it is more likely that it is La(d^2s^1) rather than La(d^1s^2) that reacts with CH_2O on both doublet and quartet PES as suggested by the 5d population of La. The main reason is that $s \rightarrow d$ excitation can enhance the bonding abilities of La. On the other hand, La shows a higher bonding capacity with other atoms in doublet species than in quartet species. As shown in Figure 2, the La atom in the doublet species can form as many as three covalent bonds (such as IM **P**), while in the quartet species it can only form one covalent bonds (such as IM **D′**). This is because the high-spin state usually means more unpaired electrons and thus less bonding electrons, which often make the species in the high-spin state less stable than their counterparts in the low-spin state.

The reaction on quartet PES also starts with complex **B′** between La and CH_2O, in which the La atom bonds with O atom via a head-on attachment. The forming of **B′** has no energy barrier, and **B′** lies 34.4 kcal mol^{-1} below the doublet reactants **A**. In this process, some electrons transfer from La atom to carbonyl ligand, as indicated by the changes of both the charges and spin densities on La and C atoms (see Table 3). At the same time, the formation of the La−O bond (2.132 Å) substantially weakens the C═O bond (lengthened to 1.327 Å).

Then, La inserts into one C−H bond via TS **C′**, forming IM **D′**. In quartet **C′**, the C−H bond (2.512 Å) is completely broken, accompanied by the formation of a La−H (2.082 Å) single bond. Compared to the doublet **D**, the LaH moiety bonds with the CHO moiety by a much weaker d−π interaction. In **D′**, the La−O distance (2.317 Å) is much shorter than the La−C distance (2.630 Å) owing to La's oxophilicity. From **B′** to **D′**, the electron continues to flow from La to the carbonyl ligand as well as the H atom bonded to La. Therefore, this step can be viewed as an oxidative addition, the same nature as the first C−H insertion in doublet PES.

If one starts from IM **D′**, there are two competing pathways to form two more stable intermediates (**K′** and **J′**), respectively,

and both intermediates finally dissociate into H_2 and quartet LaCO.

D′ converts to **R′** through TS **F′**. The barrier corresponding to **F′** (15.1 kcal mol^{-1}) is much lower than that corresponding to **F** (44.0 kcal mol^{-1}), but **F′** is still 12.2 kcal mol^{-1} higher in energy than **F** because the parent **D′** is 41.1 kcal mol^{-1} higher than **D**. **F′** is close to **F** in geometry, except that the C−H bond in the former (1.235 Å) is 36% shorter than that in the latter (1.683 Å), while the H−H bond in the former (1.337 Å) is 30% longer than that in the latter (1.030 Å), indicating that **F′** is an early transition state while **F** is a late transition state. From **F′**, a stable complex **R′** is directly formed, which is a weakly bound complex between LaCO and H_2 with a side-on bonding of H_2. The planar structure, obtained by directly breaking the C−H bond in TS **F′**, however, is not an intermediate but a TS with an imaginary frequency of 132 cm^{-1} for the twisting of H_2 moiety. IRC analysis indicates that **R′** needs to adopt an asymmetric conformation[36] before its isomerization to the end-on carbonyl complex **J′**. As a weakly bound complex of the side-on H_2 moiety and the quartet LaCO moiety, **J′** can easily decompose into H_2 and LaCO($^4\Sigma$). During the continuous transformations from **D′** to **M′**, the La−H bond is gradually weakened, causing electrons to flow back from H atom to La atom. Besides the quartet end-on LaCO compound **J′**, **R′** can also form a quartet side-on La(η^2-CO) compound via direct loss of H_2; yet La(η^2-CO) will ultimately convert into LaCO, similar to its doublet counterpart.

D′ can also convert to **I′** through an asymmetric TS **G′** in which the dihydrogen group is nearly coplanar with La and C by an 11.9° H−La−C−H′ dihedral angle. The barrier from **D′** to **G′** is 3.4 kcal mol^{-1} higher than that from **D′** to **F′** and the resulting IM **I′** is 2.4 kcal mol^{-1} higher than IM **R′**, implying that **D′** → **I′** is less favorable than **D′** → **R′** for the second C−H insertion. However, **R′** and **I′** are both weakly bound complexes between La(η^2-CO) and H_2, just differing in the conformation of the dihydrogen group, and these weak complexes all have similar energies. The side-on carbonyl ligand in **I′** can easily convert to a terminal ligand via TS **T′**. A quartet carbonyl(η^2-dihydrogen)lanthanum (**K′**) is thus formed. As a weak complex of H_2 and LaCO($^4\Sigma$), it is also easy for **K′** to lose H_2 directly.

3.3.3. Doublet−Quartet Crossing. Because quartet **F′** and doublet **F** have similar geometries and the resulting quartet **R′** is 4.3 kcal mol^{-1} lower than doublet **R**, the **F′** → **R′** step is most likely to be involved in spin crossing with the **F** → **R** step. To better understand the property of the crossing seam between the two potential energy surfaces, we employ the same approach as proposed by Yoshizawa et al.[37] The main idea of the approach is to evaluate energy-minimum and -maximum crossing points by performing a series of single-point computations in one spin state on the basis of the geometrical changes along the IRC in another spin state and vice versa. It should be noted that the crossing points obtained in this way cannot tell us the precise energy and structure of lowest energy crossing point though it provides a reasonable range of the crossing seam.[37]

The solid and the dotted lines in Figure 3a depict the potential energy profiles of the doublet and the quartet PES, respectively, on the basis of the geometries located along the doublet IRC. As shown in Figure 3a, the crossing point CP1 is located in the very vicinity of no. 6 point[36] with energy of −19.7 kcal mol^{-1} relative to the initial doublet reactants at the ZORA-BP86/TZ2P level. This point, whose geometry is close to that of **R**, has a dissociating C−H bond of 2.098 Å and a forming H−H bond

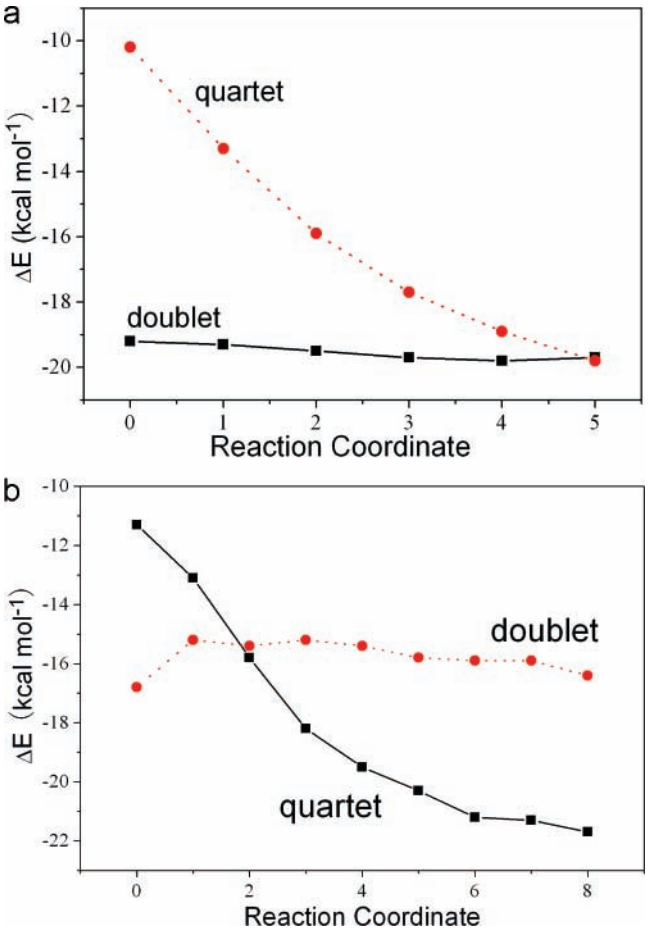

Figure 3. Profiles of the potential energy surface crossing: (a) profile based on the geometrical change along the doublet IRC; (b) profile based on the geometrical change along the quartet IRC.

of 0.845 Å. The doublet and the quartet PES cross at this point, and thus, the reaction may jump from the doublet PES to the quartet PES near CP1 resulting in a low-energy reaction pathway toward products. Therefore, CP1 can be viewed as the energy-minimum crossing point between the two potential energy surfaces regarding the H atom transfer. Similarly, CP2 can be found in the very vicinity of no. 3 point[36] along the quartet IRC as shown in Figure 3b. This point is −15.9 kcal mol^{-1} below the reactants at the ZORA-BP86/TZ2P level, with a breaking C−H bond of 1.552 Å and a forming H−H bond of 0.910 Å. The estimated CP2 is the energy-maximum crossing point. Thus, there would be a crossing region between CP1 and CP2 where the reaction system is most likely to jump from doublet to quartet PES.

We also investigate some other possible crossing regions. It is noticed that **I′** → **K′** has similar geometric change as **R** → **J**, and the former crosses with the latter twice in energy changes. However, no crossing points are found in this region through the same approach as used above, suggesting that there may be no spin conversion in this region from quartet state to doublet state and vice versa. In addition, there is probably some spin crossing in the region of **K** → **L** → **M** and **J′** → **M′** because the weakly bound complexes of H_2 and LaCO in both doublet state and quartet state are quite close in energies and geometries.[36]

Our discussion on the production of H_2 and LaCO can be summarized as that reaction system may jump from doublet to quartet states in the vicinity of (η^2-H_2)La(η^2-CO) to form intermediates more stable toward H_2 and quartet LaCO.

3.4. Reaction Pathway to H + LaCHO. Besides a second C−H insertion to form dihydro complexes (**K** and **J**), IM **D** can also directly form formyllanthanum by losing a H atom. This reaction is highly endothermic ($\Delta E_{DK} = 61.0$ kcal mol^{-1}), and the products are 16.5 kcal mol^{-1} higher than the initial reactants; therefore, it is an unfavorable reaction pathway, similar to the formation of formylyttrium.[12] It should be noted here that the electronic ground state of the product formyllanthanum is in triplet state rather than in singlet state. In triplet LaCHO, La has an electron population similar to that in the parent HLaCHO as indicated by the Mulliken population analysis.

3.5. Reaction Pathway to LaO + CH_2. Due to the high oxophilicity of La, insertion of a La atom into the C═O bond is entirely possible. As shown in Figure 2, the C−O bond can be dissociated by La atom via TS **O**, resulting in the most stable complex **P** on the doublet PES ($\Delta E_{AP} = -71.1$ kcal mol^{-1}). The barrier for the C−O insertion is 27.0 kcal mol^{-1}, slightly smaller than that for the C−H insertion. As shown in Table 2, during the forming of the La−O and La−C bond as well as the breaking of the C−O bond, an electron transfers from La atom to C atom, resulting in spin-paired La (spin density, 0.09) and unsaturated C (spin density, 0.91). The La−C distance in **P** is 2.515 Å, indicating a single La−C bond. The La−O distance in **P** is only 0.026 Å longer than that of the free LaO. Such geometric characteristics indicate that **P** is more likely a complex between LaO and CH_2 than a complex between O and $LaCH_2$. Orbital analysis for **P** indicates that the La−C single bond is formed by the SOMO (σ^1) of LaO ($\sigma^2\pi^4\sigma^1$)[38] and the SOMO (a_1) of CH_2 ($a_1^2b_2^2a_1^1b_1^1$). Therefore, the resulting SOMO is located on the C atom rather than on the La atom; this bonding character is a feature distinctive from other intermediates and may be utilized for the elongation of carbon chain via reactions of **P** with other organic molecules. Meanwhile, it is difficult for **P** to dissociate into LaO and CH_2 (**Q**) because the process is rather endothermic ($\Delta E_{QR} = 79.1$ kcal mol^{-1}); thus, LaO + CH_2 are also the minor products of the reaction between La and CH_2O.

3.6. Electronic Structures of MCO (M = Sc, Y, La, Ce, Gd, and Lu) and Their Implications on the Reaction Mechanisms between M and CH_2O. Since lanthanum and yttrium are both in group III and both have the same valence electronic structure ($n-1$)d^1ns^2, they are supposed to have much in common in the reaction with formaldehyde, as has been discussed above. However, the huge difference in the ns → ($n-1$)d promotion energy leads to two different reaction patterns in the formation of a metal−carbonyl compound: For La, the ground state of LaCO is quartet state, while the ground state of the reactants is a doublet state, suggesting a PES of high spin state must be involved and thus spin conversion must occur in some region; for Y, the ground state of YCO is doublet state, suggesting a high spin state may not need to be involved. Moreover, the MCO compound (M = Sc, Y, La, Ce, Gd, and Lu) can be sorted into two groups since these elements have the same d^{1}s^2 valence electron configurations but different s → d promotion energies (see Table 4): one is in low-spin state (like YCO), including YCO and LuCO; the other is in high-spin state (like LaCO), including ScCO, LaCO, CeCO,[39] and GdCO.[40] Consequently, formation of MCO can also be grouped into a YCO-like mechanism that may involves only low-spin state and LaCO-like mechanism that involves high-spin state as well as low-spin state.

Here we mention an interesting phenomenon that Sc and Y have similar s → d promotion energies but the ground states of their carbonyl complexes are different. The ground state of ScCO($^4\Sigma$) has been well-confirmed by electron spin resonance (ESR) spectroscopy[41] as well as highly accurate theoretical calculation.[42] However, no clear ESR experimental evidence for the ground state of YCO has yet been reported, and available theoretical studies have not given a unified answer to the question either. In the computational work of Jeung,[43] only the high-spin state of YCO has been considered, while, in the work of Siegbahn,[44] it only mentioned that "the yttrium atom also uses its s^2-state to form the bond of Y(CO)". Meanwhile, our own DFT calculations predict a ν(CO) frequency for YCO($^2\Pi$) at 1930 cm^{-1}, which is in line with the experimentally observed frequencies (1874.1 and 1869 cm^{-1}) as assigned by Zhou et al.[45] In comparison, the computed ν(CO) frequency for YCO($^4\Sigma$) is 1809 cm^{-1}. Thus, considering that DFT methods often overestimate vibrational frequencies, the $^2\Pi$ state is probably the most competitive candidate for the ground state of YCO and highly accurate theoretical studies are needed to clarify this problem. To understand the difference between neutral Sc and Y atoms, one can also look at their cationic carbonyl complexes for some indirect evidence. The ground state of $ScCO^+$ is the $^3\Delta$ state derived from the 3d^{1}4s^1(^{3}D) Sc^+ ground state, while the ground state of YCO^+ is the $^1\Sigma^+$ state derived from the 5s^2(^{1}S) Y^+ ground state.[46] Although d-rich configurations are favorable for the back-donation from metal to carbonyl ligand, the Y^+ ion still adopts a roughly d-free configuration to interact with CO, suggesting that the d electron is less favorable for back-donation in Y than in Sc. Anyhow, we raise some questions here and hope that this work would provide ground for further studies.

TABLE 4: Comparison of the Electronic Ground State of MCO in Which the Rare Earth Atom M All Have the Same Valence Subconfiguration d^{1}s^2

element	electronic confign of the element	PE (kcal mol^{-1})[a]	electronic confign of the MCO compd
Sc	3d^{1}4s^2	33.0	$1\pi^4 2\sigma^2 2\sigma^1 2\pi^2$
Y	4d^{1}5s^2	31.4	$1\pi^4 2\sigma^2 2\sigma^2 2\pi^1$
La	5d^{1}6s^2	7.6	$1\pi^4 2\sigma^2 2\sigma^1 2\pi^2$
Ce	4f^{1}5d^{1}6s^2	6.7	$4f^1 1\pi^4 2\sigma^2 2\sigma^1 2\pi^2$
Gd	4f^{7}5d^{1}6s^2	18.2	$4f^7 1\pi^4 2\sigma^2 2\sigma^1 2\pi^2$
Lu	4f^{14}5d^{1}6s^2	54.0	$4f^{14} 1\pi^4 2\sigma^2 2\sigma^2 2\pi^1$

[a] Promotion energy from ($n-1$)d^1ns^2 to ($n-1$)d^2ns^1.

4. Summary

Density-functional calculations, followed by correlation corrections at the CCSD(T) level, have been performed to explore the decomposition of formaldehyde in the assistance of lanthanum atom, and comparison is made to the Y + CH_2O reaction. In summary, pathways leading to four groups of products have been studied in detail:

$$La(^2D) + H_2CO \rightarrow LaH_2 + CO \quad (1)$$

$$\rightarrow LaCO(^4\Sigma) + H_2 \quad (2)$$

$$\rightarrow LaCHO + H \quad (3)$$

$$\rightarrow LaO + CH_2 \quad (4)$$

At the CCSD(T) level, group 1 products are predicted to be the most favorable products from both thermodynamic and kinetics, followed by the competing group 2 products in a high-spin state. To explain the formation of quartet LaCO, a potential energy profile in the quartet state is also mapped and the possible spin-crossing region is estimated by a simple approach. Group

3 products are the least favorable products because the products have highest energies among all the four groups of products. Pathways leading to product groups 1−3 have previously been studied for Y + CH_2O (except for the pathways in the quartet PES). In addition, a previously unexplored pathway leading to metal monoxide and a carbene radical (group 4) has also been studied in this work. Group 4 products are not major products since the parent complex $OLaCH_2$ is quite stable and the dissociation energy is also large.

The potential energy profiles obtained at the DFT level are qualitatively in good agreement with those obtained at the CCSD(T) level, except that group 2 products, instead of group 1, are predicted to be the most stable products. The discrepancies can be accounted by a previous conclusion[47] that DFT methods favor d-rich species and overestimate their bonding energies.

The major difference between La + CH_2O reactions and Y + CH_2O reactions, as mentioned above, is the involvement of the quartet PES for the former and possibly none for the latter. According to the electronic ground state of the metal carbonyl compound, the rare earth elements bearing $f^N d^1 s^2$ ground states ($N = 0$, for Sc; $N = 1$, for Ce; $N = 7$, for Gd; $N = 14$, for Lu) can be sorted into two groups: The first one involves a d^2s^1 subconfiguration bonding with CO, including Sc, La, Ce, and Gd; the second one involves a d^1s^2 subconfiguration bonding with CO, including Y and Lu. Therefore, the reaction between elements in the first group with CH_2O involves high-spin potential energy surface and the cross between the high-spin and low-spin PES, while the reaction between elements in the second group and CH_2O may not need the involvement of high-spin PES.

In summary, our study provides some new features of reactions between group III La atoms and formaldehyde, extending the previous study of Y + CH_2O reactions. We hope these results will not just advance our understanding about how early transition metals aid the dissociation of formaldehyde but also shed light on the mechanism of its reverse reaction, i.e., catalytic hydrogenation of carbon monoxide by early transition metals.

Acknowledgment. We are grateful for the fruitful discussions with Prof. Ming-Fei Zhou. This work was supported by the NKBRSF (Grant 2004CB719501) and NNSFC (Grants 20433020, 20673024) as well as the Natural Science Foundation of Shanghai Science & Technology Committee (Grants 04JC14016, 05DZ22313).

Supporting Information Available: Cartesian coordinates of selected complexes as described in the text. This material is available free of charge via the Internet at http://pubs.acs.org.

References and Notes

(1) (a) Cant, N. W.; Tonner, S. P.; D. Trimm, L.; Wainwright, M. S. *J. Catal.* **1985**, *91*, 197. (b) Klier, K. *Adv. Catal.* **1982**, *31*, 243. (c) Mazanec, T. *J. Catal.* **1986**, *98*, 115. (d) Biloen, P.; Sachtler, W. M. H. *Adv. Catal.* **1981**, *30*, 165.

(2) Atkinson, R.; Baulch, D. L.; Cox, R. A.; Hampson, R. F.; Kerr, J. A.; Troe, J. *J. Phys. Chem. Ref. Data* **1992**, *21*, 1125.

(3) Moore, C. B.; Weisshaar, J. C. *Annu. Rev. Phys. Chem.* **1983**, *34*, 525.

(4) Raskó, J.; Kecskés, T.; Kiss, J. *J. Catal.* **2004**, *226*, 183.

(5) Formaldehyde has been defined as a known human carcinogen. See the following: *Formaldehyde and Cancer*: *Questions and Answers*; http://www.cancer.gov/cancertopics/factsheet/Risk/formaldehyde and reference therein. For other health issues caused by formaldehyde, see the following: http://epa.gov/ttn/atw/hlthef/formalde.html.

(6) Lias, S. G.; Bartmess, J. E.; Liebman, J. F.; Holmes, J. L.; Levin, R. D.; Mallard, W. G. *J. Phys. Chem. Ref. Data* **1988**, *17*, Suppl. No. 1.

(7) (a) Stauffer, H.; Hinrichs, R.; Schroden, J.; Davis, H. *J. Chem. Phys.* **1999**, *111*, 10758. (b) Schroden, J. J.; Teo, M.; Davis, H. F. *J. Chem. Phys.* **2002**, *117*, 9258.

(8) (a) Fisher, E. R.; Armentrout, P. B. *J. Phys. Chem.* **1990**, *94*, 1674. (b) Siegbahn, P. E. M. *Organometallics* **1994**, *13*, 2833. (c) Park, M. A.; Hauge, R. H.; Margrave, J. L. *International Conference on Low Temperature Chemistry*, 2nd, Kansas City, MO, Aug 4−9, 1996; BkMk Press: Kansas City, MO, 1996, pp 203−204. (d) Hoyau, S.; Ohanessian, G. *Chem. Phys. Lett.* **1997**, *280*, 266. (e) Saendig, N.; Koch, W. *Organometallics* **1998**, *17*, 2344. (f) Damyanova, B.; Momtchilova, S.; Bakalova, S.; Zuilhof, H.; Christie, W.; Kaneti, J. *J. Mol. Struct.* (*THEOCHEM*) **2002**, *589*−*590*, 239. (g) Boutreau, L.; Toulhoat, P.; Tortajada, J.; Luna, A.; Mo, O.; Yanez, M. *J. Phys. Chem. A* **2002**, *106*, 9359. (h) Zhang, G.; Li, S.; Jiang, Y. *Organometallics* **2004**, *23*, 3656. (i) Lu, W.; Abate, Y.; Wong, T.-H.; Kleiber, P. D. *J. Phys. Chem. A* **2004**, *108*, 10661. (j) Su, Z.; Qin, S.; Tang, D.; Yang, H.; Hu, C. *J. Mol. Struct.* (*THEOCHEM*) **2006**, *778*, 41. (k) LeCaer, S.; Mestdagh, H.; Schroeder, D.; Zummack, W.; Schwarz, H. *Int. J. Mass Spectrom.* **2006**, *255*−*256*, 239. (l) Wang, Y.; Chen, X. *Chem. Phys. Lett.* **2006**, *422*, 534. (m) Wyrwas, R. B.; Yoder, B. L.; Maze, J. T.; Jarrold, C. C. *J. Phys. Chem. A* **2006**, *110*, 2157.

(9) (a) Gambarotta, S.; Floriani, C.; Chiesi-Villa, A.; Guastini, C. *J. Am. Chem. Soc.* **1982**, *104*, 2019. (b) Gambarotta, S.; Floriani, C.; Chiesi-Villa, A.; Guastini, C. *Organometallics* **1986**, *5*, 2425. (c) Thiyagarajan, B.; Kerr, M.; Bollinger, J.; Yound, V., Jr.; Bruno, W. *Organometallics* **1997**, *16*, 1331. (d) Spera, M.; Chen, H.; Moody, M.; Hill, M.; Harman, W. *J. Am. Chem. Soc.* **1997**, *119*, 12772.

(10) (a) Mckee, M.; Dai, C.; Worley, S. *J. Phys. Chem.* **1988**, *92*, 1056. (b) Mestdagh, H.; Rolando, C.; Sablier, M.; Billy, N.; Gouedard, G.; Vigue, J. *J. Am. Chem. Soc.* **1992**, *114*, 771. (c) Maseras, F.; Lledos, A.; Clot, E.; Eisenstein, O. *Chem. Rev.* **2000**, *100*, 601. (d) Wang, X.; Andrews, L. *J. Phys. Chem. A* **2000**, *104*, 9892. (e) Vayssilov, G.; Roesch, N. *J. Am. Chem. Soc.* **2002**, *124*, 3783. (f) Wang, Y.; Liu, Z.; Geng, Z.; Yang, X. *Chem. Phys. Lett.* **2006**, *427*, 271.

(11) Vannice, M. A.; Sudhakar, C.; Freeman, M. *J. Catal.* **1987**, *108*, 97.

(12) Bayse, C. *J. Phys. Chem. A* **2002**, *106*, 4226.

(13) Martin, W. C.; Zalubas, R.; Hagan, L. *Atomic Energy Levels-The Rare Earth Elements*; Natl. Stand. Ref. Data Ser. 60; Natl. Bur. Stand. (U.S.): Washington, DC, 1978. Retrieved from the following: http://physics.nist.gov/PhysRefData/Handbook/periodictable.htm.

(14) Blomberg, M.; Siegbahn, Per E. M.; Svensson, M. *J. Am. Chem. Soc.* **1991**, *113*, 7076; **1992**, *114*, 6095.

(15) Hong, G.; Lin, X.; Li, L.; Xu, G. *J. Phys. Chem. A* **1997**, *101*, 9314.

(16) Friesner, R. *Proc. Natl. Acad. Sci. U.S.A.* **2005**, *102*, 6648.

(17) (a) te Velde, G.; Bickelhaupt, F. M.; van Gisbergen, S. J. A.; Fonseca Guerra, C.; Baerends, E. J.; Snijders, J. G.; Ziegler, T. *J. Comput. Chem.* **2001**, *22*, 931. (b) Fonseca Guerra, C.; Snijders, J. G.; te Velde, G.; Baerends, E. J. *Theor. Chem. Acc.* **1998**, *99*, 391. (c) *ADF 2006.01*; SCM, Theoretical Chemistry: Vrije Universiteit, Amsterdam, The Netherlands, 2006; http://www.scm.com.

(18) Becke, A. D. *Phys. Rev. A* **1988**, *38*, 3098.

(19) Perdew, J. P.; Wang, Y. *Phys. Rev. B* **1986**, *33*, 8822.

(20) (a) Schultz, N. E.; Zhao, Y.; Truhlar, D. G. *J. Phys. Chem. A* **2005**, *109*, 4388. (b) Diefenbach, A.; de Jong, G. Th.; Bickelhaupt, F. M. *J. Chem. Theory Comput.* **2005**, *1*, 286. (c) Zhao, Y.; Truhlar, D. G. *J. Chem. Phys.* **2006**, *125*, 194101. (d) Krapp, A.; Pandey, K. K.; Frenking, G. *J. Am. Chem. Soc.* **2007**, *129*, 7596.

(21) Van Lenthe, E.; Baerends, E. J. *J. Comput. Chem.* **2003**, *24*, 1142.

(22) Van Lenthe, E.; Baerends, E. J.; Snijders, J. G. *J. Chem. Phys.* **1999**, *110*, 8943.

(23) Kohn, W.; Becke, A. D.; Parr. R. G. *J. Phys. Chem.* **1996**, *100*, 12974.

(24) Deng, L.; Ziegler, T. *Int. J. Quantum Chem.* **1994**, *52*, 731.

(25) Frisch, M. J.; Trucks, G. W.; Schlegel, H. B.; et al. *Gaussian 03*, revision C02; Gaussian, Inc.: Wallingford, CT, 2004.

(26) Scuseria, G. E.; Scheiner, A. C.; Lee, T. J.; Rice, J. E.; Schaefer, H. F., III. *J. Chem. Phys.* **1987**, *86*, 2881.

(27) Dolg, M.; Stoll, H.; Savin, A.; Preuss, H. *Theor. Chim. Acta* **1989**, *75*, 173.

(28) Cao, X.; Dolg, M. *J. Mol. Struct.* (*THEOCHEM*) **2002**, *581*, 139.

(29) Kendall, R. A.; Dunning, T. H., Jr.; Harrison, R. J. *J. Chem. Phys.* **1992**, *96*, 6796.

(30) de Jong, G. T.; Solà, M.; Visscher, L.; Bickelhaupt, F. M. *J. Chem. Phys.* **2004**, *121*, 9982.

(31) Baerends, E. J.; Branchadell, V.; Sodupe, M. *Chem. Phys. Lett.* **1997**, *265*, 481.

(32) Zhao, Y.; González-García, N.; Truhlar, D. G. *J. Phys. Chem. A* **2005**, *109*, 2012.

(33) Lombardi, J.; Davis, B. *Chem. Rev.* **2002**, *102*, 2431.

(34) Wang, X.; Chertihin, G.; Andrews, L. *J. Phys. Chem. A* **2002**, *106*, 9213.

(35) Xu, Q.; Jiang, L.; Zou, R. *Chem.—Eur. J.* **2006**, *12*, 3226.
(36) See supporting information.
(37) Yoshizawa, K.; Shiota, Y.; Yamabe, T. *J. Chem. Phys.* **1999**, *111*, 538.
(38) Wang, S.; Pan, D.; Schwarz, W. *J. Chem. Phys.* **1995**, *102*, 9296.
(39) Zhou, M. F.; Jin, X.; Li, J. *J. Phys. Chem. A* **2006**, *110*, 10206.
(40) Jin, X.; Jiang, L.; Xu, Q.; Zhou, M. F. *J. Phys. Chem. A* **2006**, *110*, 12585.
(41) Van, Zee, R. J.; Weltner, W., Jr. *J. Am. Chem. Soc.* **1989**, *111*, 4519.
(42) Koukounas, C.; Kardahakis, S.; Mavridis, A. *J. Chem. Phys.* **2005**, *123*, 074327.
(43) Jeung, G. *Chem. Phys. Lett.* **1994**, *221*, 237.
(44) Siegbahn, P. E. M. *J. Organomet. Chem.* **1995**, *491*, 231.
(45) Zhou, M. F.; Andrews, L. *J. Phys. Chem. A* **1999**, *103*, 2964.
(46) Barnes, L.; Rosi, M.; Bauschlicher, C. W., Jr. *J. Chem. Phys.* **1990**, *93*, 609.
(47) Pápai, I.; Schubert, G.; Hannachi, Y.; Mascetti, J. *J. Phys. Chem. A* **2002**, *106*, 9551.